Magnetic anisotropy of tetragonal FeCo/Pt(001) superlattices

2007 J. Phys.: Condens. Matter 19 226218

(http://iopscience.iop.org/0953-8984/19/22/226218)

IOP PUBLISHING JOURNAL OF PHYSICS: CONDENSED MATTER

J. Phys.: Condens. Matter **19** (2007) 226218 (10pp) doi:10.1088/0953-8984/19/22/226218

Magnetic anisotropy of tetragonal FeCo/Pt(001) superlattices

P Warnicke[1], G Andersson[2], M Björck[2], J Ferré[3] and P Nordblad[1]

[1] Department of Engineering Sciences, Uppsala University, Box 534, Uppsala, Sweden
[2] Department of Physics, Uppsala University, Box 530, Uppsala, Sweden
[3] Laboratorie de Physique des Solides, UMR CNRS 8502, Université Paris-Sud, 91405 Orsay, France

E-mail: pewa@angstrom.uu.se

Received 15 August 2006, in final form 16 March 2007
Published 14 May 2007
Online at stacks.iop.org/JPhysCM/19/226218

Abstract

The magnetic properties of tetragonally strained $Fe_{0.36}Co_{0.64}$ alloys in the form of FeCo/Pt(001) superlattices have been investigated experimentally. The strain was controlled by varying the individual constituent thicknesses in the range 3–10 atomic monolayers (ML), resulting in lattice-parameter ratios c/a between 1.18 and 1.31. The sample with a c/a ratio of 1.18 has a preferred out-of-plane magnetization direction and magnetic stripe domains, revealed by MFM, while samples with higher c/a ratios prefer in-plane magnetization. The strain-induced contribution to anisotropy was found to have a dominating effect. Saturation-magnetization values up to 2.31 T at room temperature were measured.

1. Introduction

Magnetic materials with high magnetocrystalline anisotropy energy (MAE) are of interest because of their applicability as permanent magnets and possible use in perpendicular magnetic recording media. Some hard magnetic materials such as $SmCo_5$ provide high MAE [1, 2], which allows thermally stable magnetic grains down to order 2.5 nm and thus potentially ultra-high storage density in longitudinal as well as perpendicular recording media. However, storage media applications of these compounds are linked to several practical challenges primarily because of the limiting write field, H_w, which is proportional to the ratio between the uniaxial MAE and the saturation magnetization (M_s). Writing heads, capable of delivering 10 MA m^{-1} fields, would for example be required in recording for $SmCo_5$ based media [3]. Thus, the implementation of a giant MAE material as a recording medium would also require a giant M_s to keep the write field at reasonable magnitudes.

Alternatively, ferromagnetic multilayers with perpendicular anisotropy could be used in perpendicular magnetic recording, because of high MAE and M_s. Such systems are also of particular interest in magneto-optical recording where the read-back process employs the

magneto-optical Kerr effect, which is more emphasized for perpendicular magnetic moments compared to moments lying in the plane [4].

Multilayers exhibiting perpendicular magnetic anisotropy have been experimentally studied [5, 6] for more than two decades, since the phenomenon was first discovered in Co/Pd [7]. This has triggered theoretical work and *ab initio* calculations of uniaxial MAE in multilayers have been made on various material combinations: Fe/Pt, Fe/Pd, Fe/Au, Fe/Ag [8]; Co/Pd, Co/Cu, Co/Ag [9]; Co/Pt, Ni/Pt, Ni/Pd, Mn/Pt, Mn/Pd [10]. According to recent *ab initio* calculations [11], tetragonally strained FeCo alloys of composition around $Fe_{0.40}Co_{0.60}$ possess giant perpendicular magnetic anisotropy together with high saturation magnetization, M_s. We have previously reported [12] that FeCo/Pt multilayers with tetragonally strained FeCo layers can show perpendicular anisotropy and high M_s. Here, the magnetic properties of an extended series of such multilayer samples are reported.

2. Experimental details

The samples were grown by dc magnetron sputtering under ultra high vacuum conditions (base pressure below 1×10^{-7} Pa) using argon as the sputtering gas. A detailed description of the growth is given elsewhere [13]. Substrates of MgO with the [001] direction perpendicular to the polished surface were annealed at 700 °C for 15 min before cooling to 330 °C. At this temperature, a buffer layer consisting of 6 Å (4 ML) Fe covered by 39 Å (20 ML) Pt was grown [14, 15]. N repetitions of FeCo/Pt bilayers were then deposited at 200 °C.

N ranges from 23 to 40, depending on the bilayer thickness, and was chosen to make the total film thickness comparable for all samples in order to avoid unwanted influence on the structural and magnetic properties from differences in lattice relaxation. Here, each sample will be referred to by its label n_{FeCo}/n_{Pt}, indicating the nominal number of monolayers of each constituent. With respect to bulk distances between (002) atomic planes, one monolayer of FeCo corresponds nominally to 1.41 Å and 1 ML of Pt to 1.96 Å in the deposition procedure. In each sample, the final Pt layer works as a cap and prevents oxidation. If this layer had a nominal thickness below 15 Å some extra Pt was added to reach this thickness. The choice of thickness combinations was made to cover both a constant strain state, n_{FeCo}/n_{Pt} ratio, and a constant interface density, $1/(n_{FeCo} + n_{Pt})$, while varying the relative amount of FeCo in the multilayers. Two of the samples do not fall into either of these two categories but contribute with additional strain states for two n_{FeCo} values already present.

The composition of the FeCo alloy was regulated by the electric power on the Fe and Co targets (99.95% purity), respectively, during the co-sputtering. The obtained chemical composition, established from Rutherford backscattering spectrometry (RBS) and x-ray photoemission spectroscopy (XPS), was 64 ± 5 at.% Co [13]. The Pt target purity was 99.99%. In this text, 'FeCo' will refer to the $Fe_{0.36}Co_{0.64}$ alloy unless otherwise stated. In order to provide a reference for lattice parameters, alloy composition and magnetic moments, a film of 1000 Å FeCo was grown under the same conditions as the multilayers. The buffer layer in this sample was 45 Å Fe, deposited at 330 °C, and the film was capped by 20 Å of Pt. A schematic picture of the multilayers is shown in figure 1.

The structure of the multilayers was investigated by x-ray reflectivity, x-ray diffraction (XRD) and reciprocal space mapping (RSM). Both Pt and MgO have fcc crystal structure and their [100] direction is along the substrate edge. FeCo bulk is bcc and has its [110] direction parallel to the [100] direction of MgO. As the FeCo layers decrease in thickness the crystal structure deforms along the Bain's path from bcc towards fcc, similar to Fe in Fe/Pt multilayers [14, 16, 17]. The crystal structure in the FeCo layers is viewed as a body centred tetragonal, i.e. originally a bcc lattice but with a tetragonal distortion such that the out-of-

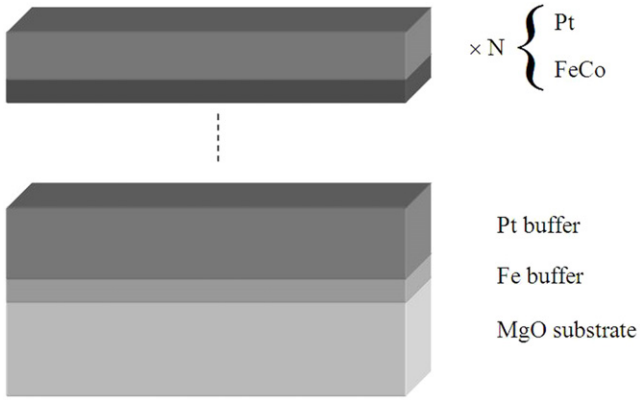

Figure 1. Structure of the prepared samples. A buffer layer of 6 Å Fe and 39 Å Pt separates the MgO(001) substrate from N repetitions of FeCo/Pt bilayers.

plane lattice parameter, c, is different from the in-plane lattice parameter, a. The distortion is quantified by the c/a ratio, where $c/a = 1$ corresponds to a body centred cubic lattice and $c/a = \sqrt{2}$ corresponds to a face centred cubic lattice. It should be noted that the interatomic distances in the FeCo layers differ from the average distances measured by XRD and RSM. All c/a values given here refer to the FeCo layers only. Details on the derivation of the individual FeCo and Pt lattice parameters are given elsewhere [13]. Concerning the bilayer thickness, the intended thickness did not deviate by more than 0.7 Å (0.5 ML FeCo) from the nominal thickness for any of the samples.

Full in-plane hysteresis loops were captured with longitudinal MOKE (LMOKE). In-plane magnetization measurements at 10 and 300 K were also carried out using a MPMS-XL SQUID (superconducting quantum interference device) magnetometer. Each sample was saturated in a high field, applied parallel to the surface. Subsequently, the applied field was decreased in settle mode (i.e. the applied field reaching stability between each measurement) until the magnetization switched to a negative value. To study the out-of-plane magnetization component, polar magneto-optic Kerr effect (PMOKE) measurements were carried out at ambient temperature. The maximum field that could be applied was 1070 kA m^{-1}. These measurements were normalized with respect to the saturation magnetization obtained by SQUID measurements. The magnetic domain structure was studied with a Nanoscope Dimension 3100 MFM (magnetic force microscope) in tapping/lift mode using standard magnetic probes.

3. Results and discussion

The set of samples is presented in table 1. All data here and in the rest of this text were obtained at 300 K, unless otherwise stated. K_{eff} and H_{s} are missing for some samples that did not reach saturation with a perpendicular configuration. In the calculation of the saturation magnetization only FeCo was assumed to give a ferromagnetic contribution. The absolute error in the measurement of the magnetization in the SQUID magnetometer (assuming a correct calibration factor and samples of similar shape) is about 1%. However, as discussed above, there is an uncertainty in the layer thickness determination that gives an uncertainty in the ferromagnetic volume of about 9%. Looking at the individual values of the saturation moments in table 1, we do not see any systematic trend with layer thicknesses and conclude that the room temperature saturation magnetization of all samples is 2.15 ± 0.17 T. However, the measured

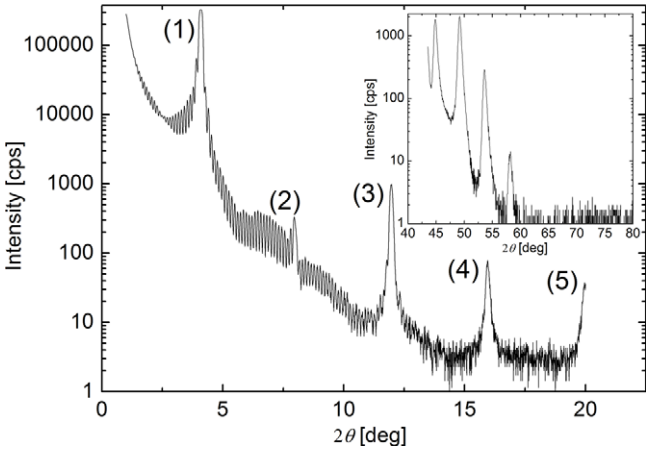

Figure 2. X-ray reflectivity and diffraction for the 8/6 sample.

Table 1. The set of multilayers prepared for this study. The first column refers to the number of monolayers for FeCo and Pt, respectively. H_c is the coercive field ($\pm$ 0.5 kA m^{-1}) and H_s the saturation field ($\pm$5 kA m^{-1}). IP and PP refer to in-plane and perpendicular-to-plane configurations. All data were obtained at 300 K, except data in the three rightmost columns obtained at 10 K.

Sample (n_{FeCo}/n_{Pt})	N	c/a	K_{eff} (MJ m^{-3})	$\mu_0 M_s$ (T)	H_c IP (kA m^{-1})	H_c PP (kA m^{-1})	H_s IP (kA m^{-1})	H_s PP (kA m^{-1})	$\mu_0 M_s$ 10 K (T)	H_c IP 10 K (kA m^{-1})	H_s IP 10 K (kA m^{-1})
3/3	40	1.31	−0.36	1.98	29	16	440	840	2.23	34	700
5/5	24	1.28	−0.56	2.25	20	10	400	750	2.56	32	490
8/8	25	1.25	—	2.00	9	2	560	—	2.23	14	720
7/3	26	1.28	−0.73	2.20	17	6	390	780	2.49	34	530
6/4	25	1.27	−0.72	2.31	19	8	300	830	2.54	30	380
4/6	23	1.24	−0.13	2.20	13	15	580	300	2.66	30	800
3/7	23	1.18	0.23	2.27	6	14	700	200	2.53	27	1200
8/6	30	1.27	—	2.04	10	4	220	—	2.21	16	220
6/9.5	25	1.26	—	2.09	8	0	240	—	2.67	18	360

temperature dependence of the saturation magnetization of each of the different samples only carries the error of the SQUID measurement. It should be noted that $\mu_0 M_s$ for 10 and 300 K differ substantially, from 8 $\pm$ 2% for the 8/6 sample up to 22 $\pm$ 2% for the 6/9.5 sample. This can be compared with $\mu_0 M_s = 2.15$ T for bulk iron, that only decreases by about 2% from 0 K to room temperature. The reference sample of 1000 Å FeCo gives a $\mu_0 M_s$ of 2.02 T at 300 K with only about 1 $\pm$ 2% decrease from 10 K. The large temperature dependence of M_s for the multilayers can be assigned to a decrease of the Curie temperature compared to bulk material, a more two dimensional magnetic character with decreasing magnetic layer thickness and a polarization [18, 19] of the Pt interlayers. We have not been able to find the parameter that systematically explains the large variation of $M_s(10\text{ K})/M_s(300\text{ K})$ with the layer thickness of FeCo and Pt. In-plane coercivity shows a tendency to decrease with increasing Pt thickness. This is more apparent for the 300 K measurements. Coercivity measurements of Co/Pt multilayers show an oscillatory dependence on Pt thickness [19] which could explain exceptions in the observed tendency.

Data from x-ray reflectivity and diffraction for the 8/6 sample is shown in figure 2. In the reflectivity data, five Bragg peaks from the chemical modulation are present up to a scattering angle of 20°, which indicates sharp interfaces between the layers. The second reflectivity Bragg peak is somewhat suppressed since the FeCo and Pt layers have almost the same thickness

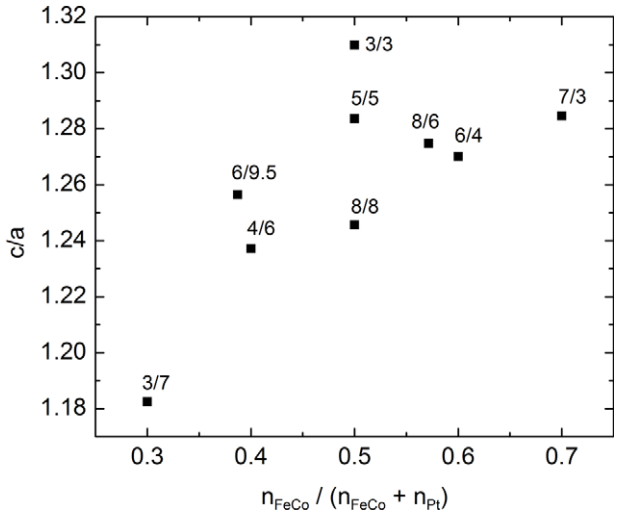

Figure 3. Strain versus relative thickness of the FeCo layer. Each sample is represented by its $n_{\mathrm{FeCo}}/n_{\mathrm{Pt}}$ label.

(nominally 11.4 Å FeCo and 11.8 Å Pt). Kiessig fringes are visible up to 12°, indicating a well defined total thickness of the superlattice. In the XRD data, the main (002) Bragg peak, corresponding to the average distance between atomic planes perpendicular to the surface, is located at 49.174°. The FWHM (full width at half maximum) of this peak is 0.513°, which implies that a lower limit of the out-of-plane coherence length is 200 Å, i.e. approximately one-third of the total thickness [20]. Satellites arising from the chemical modulation, one on the left and two on the right, are also present in the diffractogram. The intensity increase towards lower angles in the inset is due to the (002) peak of the MgO substrate, located at 42.9°. The FWHM of a rocking curve on the superlattice (002) peak yields a mosaicity of this sample of 1.1°, which is representative for all samples in the series [13].

The strain of the samples was controlled by the thickness of the constituent layers. Strain versus relative thickness of the FeCo layer is illustrated in figure 3.

In-plane MOKE and SQUID measurements along two different directions, [100] and [110], were carried out to determine the fourfold in-plane anisotropy. However, as figure 4 suggests, no substantial difference between the in-plane directions could be found. For all fabricated samples, the contribution to the fourfold in-plane anisotropy is of the order of 10^3 J m^{-3}.

In figure 5, polar and longitudinal MOKE are presented for the 6/4 sample. Here, the polar Kerr effect is one order of magnitude larger than the longitudinal. For visual clarity, both curves are plotted in units of M/M_{s}. In figure 6, the in-plane (IP) and perpendicular-to-plane (PP) magnetization versus applied field is presented for the other samples with a constant interface density. As the ratio $n_{\mathrm{FeCo}}/n_{\mathrm{Pt}}$ decreases, the preference for out-of-plane magnetization increases. For the 4/6 sample, the IP and PP magnetization curves intersect at $\mathrm{H}_A = 250$ kA m^{-1} and the saturation field, H_{s}, is twice as large for the IP compared to the PP configuration. The 3/7 sample shows magnetization curves that indicate out-of plane magnetization, which also accords with the stripe domain formation in zero field, with moments alternately pointing up and down (see figure 7).

The sample with positive effective anisotropy energy shows perpendicular domain formation with MFM. After decreasing the in-plane applied field from H_{s}, the image in figure 7 was captured at zero field and shows a stripe domain pattern with an average domain width of 150 nm. The stray fields of the magnetic domains point up and down out of the plane (represented by dark and bright regions).

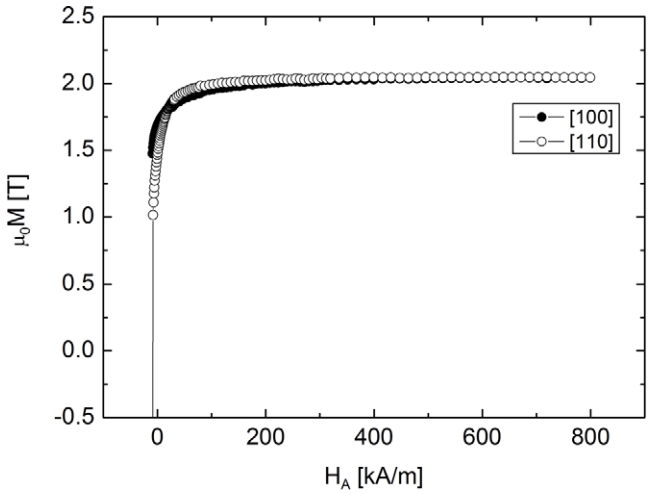

Figure 4. Magnetization versus applied field for the 8/6 sample for two different directions in plane, [100] and [110], obtained by SQUID. The small difference between the graphs reflects a weak fourfold in-plane anisotropy with [100] as the easy magnetization direction.

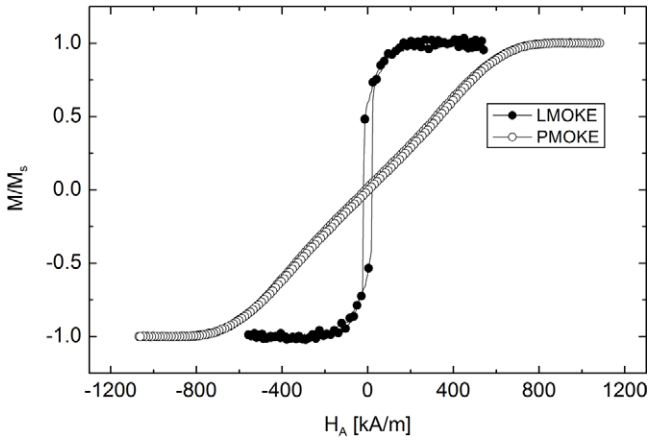

Figure 5. Longitudinal and polar MOKE for the 6/4 sample corresponding to in-plane and out-of-plane magnetization, respectively. The magnetization is normalized with respect to the saturation magnetization.

The effective anisotropy energy, approximated by $K_{\text{eff}} = K_{\text{u}} + K_{\text{d}}$, has contributions from uniaxial anisotropy, K_{u}, and demagnetization, $K_{\text{d}} = -\mu_0 M_{\text{s}}^2/2$. The latter favours in-plane alignment of the spins, which is indicated by the minus sign. K_{eff} can be determined from the area enclosed by the in-plane and out-of-plane magnetization graphs and is presented in table 1 for the samples that were possible to saturate with a PP configuration. For the 3/7 sample, $K_{\text{d}} = -2.05$ MJ m^{-3} and $K_{\text{u}} = 2.28$ MJ m^{-3}.

The effective anisotropy energy of each layer has a volume contribution K_{v} and an interface contribution $2K_{\text{s}}$ from the two interfaces enclosing the volume, according to the relation

$$K_{\text{eff}} = K_{\text{v}} + 2K_{\text{s}}/d_{\text{FeCo}}. \tag{1}$$

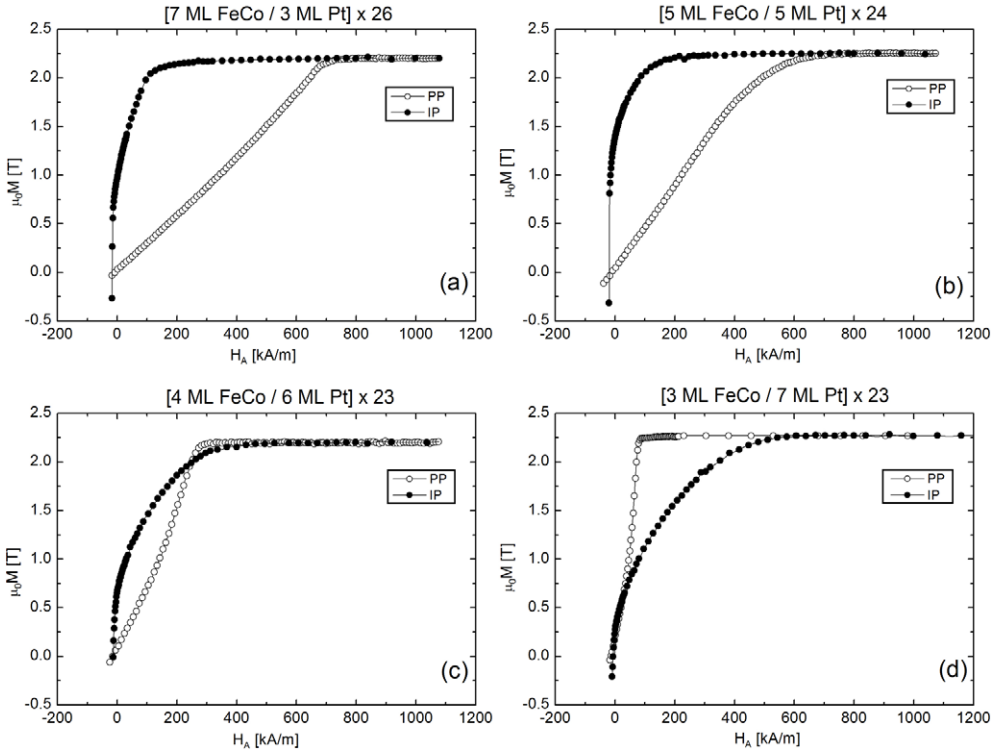

Figure 6. In-plane (IP) magnetization, obtained by SQUID, and perpendicular-to-plane (PP) magnetization, obtained by PMOKE. As shown in (a) and (b), samples 7/3 and 5/5 clearly favour magnetization in plane. Sample 4/6, illustrated in (c), is more easily saturated out of plane although having a negative K_{eff}. In (d) the 3/7 sample exhibits an out-of-plane easy axis and has a positive K_{eff}.

K_{v} consists of the demagnetization term, K_{d} defined above, and a strain induced uniaxial anisotropy K_{vu}. The term K_{vu} is expected to depend on the size of the tetragonal lattice distortion, c/a, and is from theoretical calculations [11] found to be largest for $c/a \approx 1.24$. However, to straightforwardly analyse the behaviour, we first assume that K_{vu} is constant for our samples, which represent c/a values from 1.18 to 1.31.

In figure 8, $K_{\text{eff}}d_{\text{FeCo}}$ versus the layer thickness, d_{FeCo}, is plotted together with a linear fit for samples with a constant interface density (represented by squares). The volume contribution is given by the slope and is $K_{\text{v}} = -1.5$ MJ m^{-3}. Here, the negative sign indicates in-plane preference. The interface contribution, K_{s}, is obtained from the intersection with the vertical axis $d_{\text{FeCo}} = 0$ and equals 0.38 mJ m^{-2}. This term favours out-of-plane magnetization and dominates for $d_{\text{FeCo}} < 0.5$ nm, corresponding to 3.5 ML. As a comparison, we quote some earlier results from similar analyses, where it was found that K_{s} is 0.31 mJ m^{-2} for Co(001)/Pt(001) on glass substrates [21], and $K_{\text{s}} = 0.47$ mJ m^{-2} and $K_{\text{v}} = -2.8$ MJ m^{-3} for Fe(001)/Pt(001) with $d_{\text{Fe}} < 8$ Å on Si(111) substrates [17]. Data for the 3/3 sample is plotted as a triangle but is not included in the fit. Its deviation from the overall trend of the data will be discussed below.

To get a rough estimate of the magnitude of the volume contribution, K_{vu}, from these data, we use the value of $K_{\text{v}} = -1.5$ MJ m^{-3} derived above and the average value of the saturation magnetization for the five samples included in the fit of figure 8 to estimate

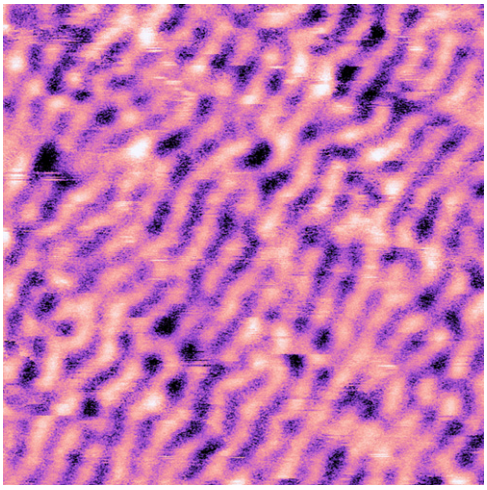

Figure 7. MFM image, 2.5 μm × 2.5 μm, captured in zero applied field showing stripe domain formation in sample 3/7. The average width of each domain is 150 nm.
(This figure is in colour only in the electronic version)

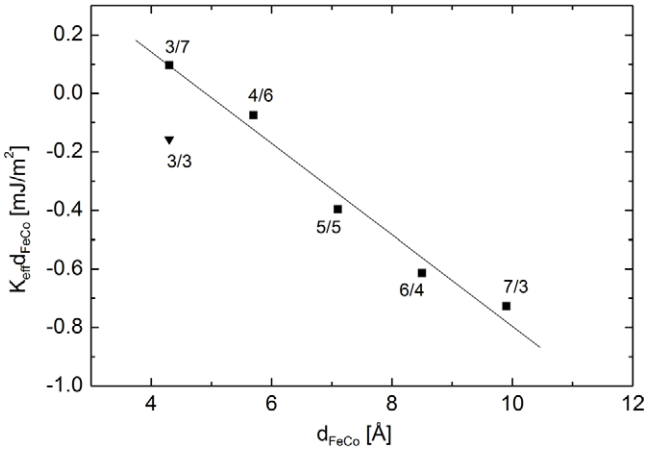

Figure 8. Anisotropy energy dependence on the individual FeCo layer thickness. Samples with a constant interface density are represented by squares. The 3/3 sample is represented by a triangle. A linear fit is made with respect to samples with a constant interface density.

$K_d \approx -2.0$ MJ m^{-3}, which yields $K_{vu} \approx 0.5$ MJ m^{-3}. These results indicate that K_s gives the largest contribution to the out-of-plane anisotropy of the 3/7 FeCo/Pt multilayer.

The above analysis assumes as mentioned a constant strain-induced anisotropy, K_{vu}. However, a strain dependence of the uniaxial anisotropy is clearly indicated by figure 9. In order to take this effect into account, equation (1) can be modified by adding the strain contribution, K_{strain}, to the bulk anisotropy energy, K_v. A quadratic relationship is assumed between the c/a ratio and the uniaxial anisotropy energy:

$$K_u = K_{vu} + K_{strain} + 2K_s/d_{FeCo},$$
$$K_{strain} = K_{c/a}\left((1-\sqrt{2})\left(\frac{c}{a}\right)^2 + \left(\frac{c}{a}\right) + \sqrt{2} - 2\right). \quad (2)$$

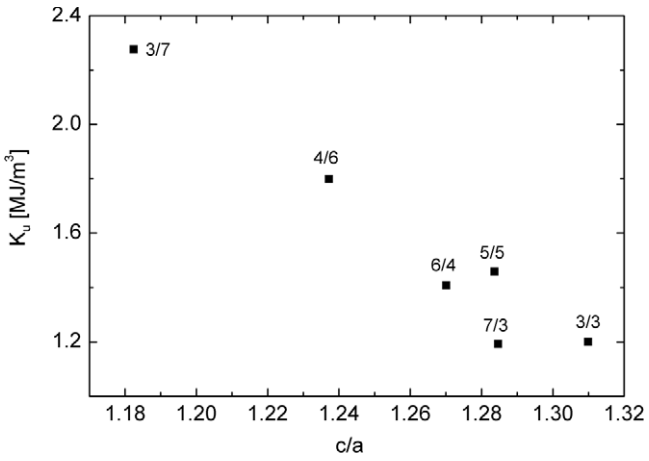

Figure 9. Dependence of uniaxial anisotropy on the strain parameter c/a.

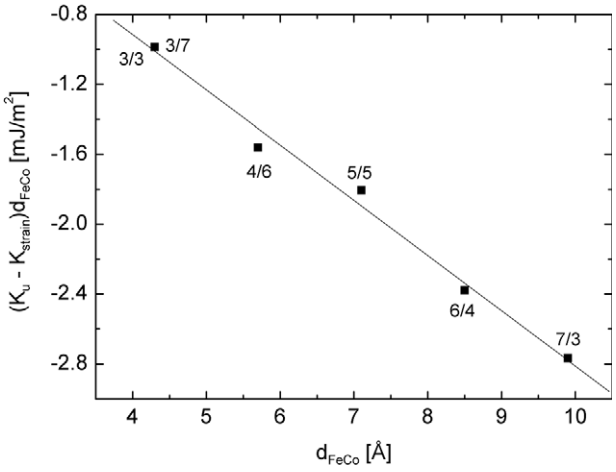

Figure 10. Determination of K_{vu} and K_s. The solid line represents a linear fit for which the slope and intersection with $d_{FeCo} = 0$, respectively, give $K_{vu} = -3.16$ MJ m^{-3} and $K_s = 0.17$ mJ m^{-2}.

Here, $K_{c/a} = 260$ MJ m^{-3} represents the contribution to the anisotropy energy coming from a change in the c/a ratio and can be approximated from the change in K_u for samples of constant FeCo thickness, i.e. samples 3/3 and 3/7. In order to validate the use of equation (2) and extract the two remaining parameters, K_{vu} and K_s ($K_u - K_{strain}$), d_{FeCo} versus d_{FeCo} is shown in figure 10. It should be noted that this model explains the low value for the 3/3 sample seen in figure 8. From the linear fit $K_{vu} = -3.16$ MJ m^{-3} and $K_s = 0.17$ mJ m^{-2} were determined. Accordingly, K_s has been reduced to about half of the value obtained with the previous model. This suggests that the large portion of apparent interface contribution calculated using equation (1) instead stems from a strain contribution, as supported by the discussion in [4]. This model gives null strain anisotropy contribution for bcc ($c/a = 1$) and fcc ($c/a = 1.44$) alloys and a maximum for $c/a = 1.21$. The theoretically calculated [11] K_{vu} shows a maximum for $c/a \approx 1.24$.

4. Conclusions

A series of FeCo/Pt multilayers has been fabricated and investigated experimentally. The $Fe_{0.64}Co_{0.36}$ layers are found to be tetragonally strained with c/a values in the range 1.18 to

1.31. Uniaxial perpendicular anisotropy is induced by the strain. A simple analysis of the thickness dependence of the measured effective anisotropy indicates that interface anisotropy gives the dominant contribution to the out-of-plane anisotropy for samples with very thin FeCo layers. However, further analysis with a model including the dependence of the anisotropy on the magnitude of the tetragonal strain in the layers reveals that a major part of the apparent interface anisotropy originates from strain rather than the interfaces. This agrees qualitatively with theoretical calculations, which indicate that the uniaxial anisotropy of the investigated alloys should be exceedingly high and strongly dependent on the strain, although the magnitude of the uniaxial anisotropy is found to be one-quarter of the value predicted from first-principles theory [11] for similarly strained FeCo alloys. Nevertheless, these calculations indicate a high sensitivity of the anisotropy to alloy composition and strain, which can explain the lower experimental values.

Acknowledgments

We gratefully acknowledge financial support from the Swedish Research Council (VR), the Swedish Foundation for Strategic Research (SSF), the Royal Physiographic Society in Lund, the Swedish Foundation for International Cooperation in Research and Higher Education (STINT) and the Göran Gustafsson Foundation. We thank one of our referees for suggesting the quadratic strain dependence of anisotropy.

References

[1] Benz M G and Martin D L 1970 *Appl. Phys. Lett.* **17** 176
[2] Herbst J F and Croat J J 1991 *J. Magn. Magn. Mater.* **100** 57
[3] Weller D, Moser A, Folks L, Best M E, Lee W, Toney M, Schwickert M, Thiele J U and Doerner M 2000 *IEEE Trans. Magn.* **36** 10
[4] Johnson M T, Bloemen P J H, den Broeder F J A and de Vries J J 1996 *Rep. Prog. Phys.* **59** 1409
[5] Tsunashima S 2001 *J. Phys. D: Appl. Phys.* **34** R87
[6] Heinrich B and Cochran J F 1993 *Adv. Phys.* **42** 523
[7] Garcia P F, Meinhaldt A D and Suna A 1985 *Appl. Phys. Lett.* **47** 178
[8] Kyuno K, Yamamoto R and Asano S 1992 *Modelling Simul. Mater. Sci. Eng.* **1** 133
[9] Daalderop G H O, Kellyand P J and Schuurmans M F H 1990 *Phys. Rev.* B **41** 11919
[10] Ravindran P, Kjekshus A, Fjellvåg H, James P, Nordström L, Johansson B and Eriksson O 2001 *Phys. Rev.* B **63** 144409
[11] Burkert T, Nordström L, Eriksson O and Heinonen O 2004 *Phys. Rev. Lett.* **93** 027203
[12] Andersson G, Burkert T, Warnicke P, Björck M, Sanyal B, Chacon C, Zlotea C, Nordström L, Nordblad P and Eriksson O 2006 *Phys. Rev. Lett.* **96** 037205
[13] Andersson G, Björck M, Lidbaum H, Sanyal B, Chacon C, Zlotea C and Valizadeh S 2007 *J. Phys.: Condens. Matter* **19** 016008
[14] Han K, Yu-Zhang K, Kung H, Embury J D, Daniels B J and Clemens B M 2002 *Phil. Mag.* A **82** 1633
[15] Mewes T, Rickart M, Mougin A, Demokritov S O, Fassbender J, Hillebrands B and Scheib M 2001 *Surf. Sci.* **481** 87
[16] Sakurai M, Imamura N and Shinjo T 1995 *J. Magn. Magn. Mater.* **147** 16
[17] Sakurai M 1994 *Phys. Rev.* B **50** 3761
[18] Giessler J, Goering E, Justen M, Weigand F, Schütz G, Langer J, Schmitz D, Maletta H and Mattheis R 2001 *Phys. Rev.* B **65** 020405
[19] Knepper J W and Yang F Y 2005 *Phys. Rev.* B **71** 224403
[20] Fewster P F 2003 *X-ray Scattering from Semiconductors* 2nd edn (London: Imperial College Press)
[21] Lin C J, Gorman G L, Lee C H, Farrow R F C, Marinero E E, Do H V, Notarys H and Chien C J 1991 *J. Magn. Magn. Mater.* **93** 194